Human Joint Angle Estimation with Inertial Sensors and Validation with A Robot Arm

Mahmoud El-Gohary, and James McNames

***Abstract*—Traditionally, human movement has been captured primarily by motion capture systems. These systems are costly, require fixed cameras in a controlled environment, and suffer from occlusion. Recently, the availability of low-cost wearable inertial sensors containing accelerometers, gyroscopes, and magnetometers have provided an alternative means to overcome the limitations of motion capture systems. Wearable inertial sensors can be used anywhere, cannot be occluded, and are low cost. Several groups have described algorithms for tracking human joint angles. We previously described a novel approach based on a kinematic arm model and the Unscented Kalman Filter (UKF). Our proposed method used a minimal sensor configuration with one sensor on each segment. This article reports significant improvements in both the algorithm and the assessment. The new model incorporates gyroscope and accelerometer random drift models, imposes physical constraints on the range of motion for each joint, and uses zero-velocity updates to mitigate the effect of sensor drift. A high-precision industrial robot arm precisely quantifies the performance of the tracker during slow, normal, and fast movements over continuous 15 minute recording durations. The agreement between the estimated angles from our algorithm and the high-precision robot arm reference was excellent. On average, the tracker attained an RMS angle error of about 3° for all six angles. The UKF performed slightly better than the more common Extended Kalman Filter (EKF).**

***Index Terms*—Inertial Measurement Units, Inertial sensors, Kinematics, Joint Angle Tracking, Shoulder, Elbow.**

I. Introduction

THE need to characterize normal and pathological human movement has consistently driven researchers to develop new rigorous tracking systems. These systems need to be accurate, unobtrusive, and suitable for continuous monitoring over long periods while subjects perform normal daily activities.

Magnetic resonance imaging-based methods for measuring the mechanics of human joints have been successfully applied to evaluate biomechanics in different human joints [1], [2]. Bey *et al.* developed and validated a tracking technique for measuring glenohumeral joint translations during shoulder motion from x-ray images [3]. These systems require a dedicated laboratory, trained staff to operate the systems, and are restricted to static or very slow and limited range of motion. Tracking of bone pins has also been used, but this is an invasive technique which limits the number of subjects who might be willing to participate in these studies [4], [5]. Motion capture systems have been successfully used to quantify joint kinematics by tracking the position of reflective surface markers during dynamic activities [6]. However, these systems are costly, restricted to controlled laboratory settings, suffer from occlusion, and are susceptible to skin movement artifact; all of which limit their usage [7].

To overcome many of the limitations associated with conventional motion measurement techniques, inertial measurement units (IMU) consisting of triaxial accelerometers were used to estimate thigh, shank and knee pitch and yaw angles [8], [9]. These studies were limited to measuring only 2 degrees of freedom (DOFs) movement during limited activities.

Most studies using IMU's, combine accelerometers and gyroscopes in wearable sensor systems [10], [11]. Traditionally, the orientation of a segment has been estimated by integrating the angular velocities measured by gyroscopes and position is obtained by double integration of the translational acceleration measured by accelerometers. A significant problem with integration, however, is that inaccuracies inherent in the measurements quickly accumulate and rapidly degrade accuracy. Roetenberg showed that integration of noisy gyroscope data resulted in a drift between $10 - 25^\circ$ after one minute [12]. Roetenberg *et al.* argued that errors due to magnetic field disturbance may be compensated by adequate model-based sensor fusion [13]. They developed a Kalman filter that operated on two inputs: the difference between inclination from the accelerometer and gyroscope, and from the magnetometer and gyroscope. The states of the model included the gyroscope bias error, orientation error, and magnetic disturbance. The filter was tested with ferromagnetic materials close to the sensor for less than a minute. The results show that the orientation estimates improved significantly when the magnetic interference correction was used. However, the accuracy could decrease if the magnetic disturbance was due to varying sources that are present during longer periods of testing.

To reduce the effect of gyroscope drift on orientation estimates, accelerometers and magnetic sensors have been used to compensate the drift about the horizontal plane, and the vertical axis respectively [14], [15]. Favre *et al.* integrated angular velocity data and corrected angle estimates based on known joint anatomical constraints and inclination data from accelerometers during static periods [16]. Luinge *et al.* used physical constraints in the elbow to measure the forearm orientation relative to upper arm [17], [18]. They minimized the error around the vertical axis by using the knowledge that the elbow joint does not permit abduction/adduction movement. Although they reported an improvement in estimating the orientation, the average orientation error was 20°. Cooper *et al.* also used biomechanical constraints to estimate knee joint flexion/extension with 2 IMU's with triaxial accelerometers and gyroscopes attached to the thigh and shank. The performance of the algorithm was evaluated with data obtained from

El-Gohary (mahmoud@apdm.com), McNames and PSU have a significant financial interest in APDM, a company that may have a commercial interest in the results of this research and technology. The potential individual and institutional conflicts of interest have been reviewed and managed by PSU.

7 healthy subjects during walking and running over 5 minute periods. The average measurement error ranged from $0.7°$ for slow walking to $3.4°$ for running [19]. However, the algorithm only used a simplified model of a single hinge knee joint.

In other studies, systems with accelerometers, gyroscopes and magnetometers were used to measure the orientation of different body segments [20]–[24]. Accelerometer and gyroscopes were used to estimate inclination and orientation. Magnetometers were used to measure orientation around the vertical axis, assuming uniform local magnetic field. Bachmann *et al.* investigated the effect of magnetic disturbance on the accuracy of orientation tracking systems and observed errors that ranged from $12°$ to $16°$ [25]. Yun *et al.* presented a simplified algorithm for orientation estimation using only accelerometers and magnetic field measurements [26]. The gyroscope-free system was only suitable for tracking slow movements. Cutti *et al.* used inertial and magnetic data to measure arm kinematics in one subject performing tasks involving shoulder and elbow single-joint-angle movements [27] and obtained an average $\mathrm{RMSE} \leq 3.6°$.

In summary, other groups have used accelerometers and magnetometers to compensate for the orientation error that occurs when integrating the angular rate from gyroscopes, but all of these methods were only applicable under limited circumstances. Some groups restricted the application to simple tasks and short tracking periods. In other studies, the estimation was accurate for only brief periods when the acceleration measurements were only due to gravity. Others reported large orientation errors due to magnetic field disturbances.

In a previous study [28], we combined kinematic models designed for control of robotic arms with state space methods to estimate human joint angles using two wearable inertial measurement units. Each IMU consisted of triaxial gyroscopes and accelerometers. We used the unscented Kalman filter (UKF) to estimate shoulder and elbow joint angles from eight subjects performing prescribed and free arm articulation for an average of 2 minutes. Compared to angles obtained from an optical reference system, we achieved an RMS angle error of less than $8°$. Although errors between optical and inertial angle estimates are minimal, some of these errors might be attributed to markers moving independently of each other, especially during fast movements [29]. Tracking performance is also limited by the noise and drift of MEMS inertial sensors.

In this study, we incorporate sensor random drift models, prior knowledge of physical constraints and human natural range of motion to obtain better joint angle estimates, and to mitigate the effect of sensors drift on the estimated angles during long periods of movement. We also employ zero-velocity updates to mitigate the effect of gyroscope drift on the estimated heading angles. We quantify the performance of our UKF-based method by comparing the angle estimates to those obtained directly from a 6-axis high-precision robot during 15-minute recordings for slow, regular and fast-speed arm movement. We evaluate the performance of the extended Kalman filter (EKF) compared to that of the UKF in estimating the joint angles, given the nonlinear relationship between the joint angles and the sensor measurements.

II. Theory

To describe angles and movements of an arm segment relative to its neighboring segments, we use an established method of biomechanical modeling based on a sequence of links connected by joints. This method was proposed by Denavit and Hartenberg in 1955, and has been used in the analysis and control of robotic manipulators [30]. The method is based on characterizing the relationship between links and joints with a (4×4) homogeneous transformation matrix. The matrix depends on four parameters associated with each link. The first parameter is the link length a_i which is the distance from the rotation axis Z_i to Z_{i+1} measured along their common normal axis X_i. The link twist α_i, is the angle from Z_i to Z_{i+1} measured about the X_i axis. The distance from X_{i-1} to X_i measured along the Z_i axis is known as the link offset d_i. The fourth parameter is the joint angle θ_i, which is the angle from X_{i-1} to X_i measured about the Z_i axis. These four parameters are known as the Denavit-Hartenberg (D-H) parameters and will be specified for the 6 DOFs arm model in the following section. To describe the kinematics of each link relative to its adjacent link, it simplifies this description to attach a frame to each link. The convention of attaching frames to the arm was detailed in [31].

A. Arm joint angles

We present a model for an arm movement with six degrees of freedom. Typically, the shoulder joint is modeled as a ball-and-socket joint with three DOFs. However, for the purpose of quantifying the performance of our algorithm, we model the shoulder with only two DOFs to match those of the industrial robot used in this study for comparison. Fig. 1 shows the arm model with static base reference frame 0 at the center of the shoulder joint. Frame 1 represents shoulder internal/external rotation, and frame 2 represents shoulder flexion/extension. The elbow joint is a hinge joint that allows movement in one plane, flexion/extension, represented by frame 3. The fourth joint is a pivot joint that allows for the forearm pronation/supination, and is represented by frame 4. Frames 5 and 6 represent wrist flexion/extension, and twist respectively.

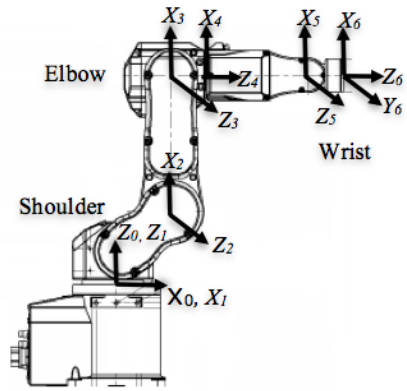

Fig. 1. Kinematics diagram of the arm model with Frame 0 as the static reference at the base. Frames 1 and 2 represent shoulder internal/external rotation, and flexion/extension, respectively. Frame 3 represents elbow flexion/extension. Frame 4 represents forearm pronation/supination. Wrist flexion/extension, and wrist twist are represented by frames 5 and 6, respectively.

Table I shows the D-H parameters of the arm model, where l_{u} is the length of the upper arm, l_{f} is the length of the forearm, and θ_i is the i^{th} angle of rotation.

TABLE I
DENAVIT-HARTENBERG PARAMETERS FOR THE 6 DOFS ARM MODEL.

Frame	α_{i-1}	a_{i-1}	d_i	θ_i
1	0	0	0	θ_1
2	$\pi/2$	a_1	0	$\theta_2 + \pi/2$
3	0	l_{u}	0	θ_3
4	$\pi/2$	0	0	$\theta_4 + \pi/2$
5	$-\pi/2$	0	l_{f}	$\theta_5 - \pi/2$
6	$\pi/2$	0	0	θ_6

We used three inertial measurement units (IMUs) to track the arm movement. Two IMUs, with triaxial gyroscopes and accelerometers, were secured with Velcro straps to the robot upper arm and forearm, and a third unit was secured inside a box on the wrist; see Fig. 2.

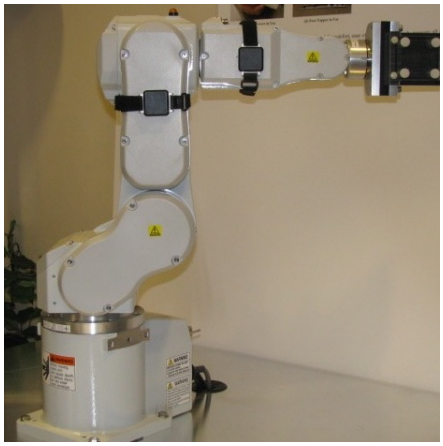

Fig. 2. Two IMUs were secured with Velcro straps to the robot upper arm and forearm, and a third unit was secured inside a box on the wrist

B. Propagation of velocity and acceleration

To formulate the dynamic equations for arm sensor measurement, including gyroscope and accelerometer data, we use three of the Newton-Euler equations of motion. Each link of the arm in motion has some angular velocity, angular and linear acceleration $(\omega, \dot{\omega}, \dot{v})$. The velocity ${}^{i+1}\omega_{i+1}$ of link $i+1$ is that of link i plus the new velocity component added by joint $i+1$. Similarly, the angular and linear acceleration of each link are related by the following recursive equations:

$$ {}^{i+1}\omega_{i+1} = {}^{i+1}_{i}R\ {}^{i}\omega_i + \dot{\theta}_{i+1}\ {}^{i+1}Z_{i+1} \tag{1} $$

$$ {}^{i+1}\dot{\omega}_{i+1} = {}^{i+1}_{i}R\,{}^{i}\dot{\omega}_i + {}^{i+1}_{i}R\ {}^{i}\omega_i \times \dot{\theta}_{i+1}\ {}^{i+1}Z_{i+1} + \ddot{\theta}_{i+1}\ {}^{i+1}Z_{i+1} \tag{2} $$

$$ {}^{i+1}\dot{v}_{i+1} = {}^{i+1}_{i}R\left[{}^{i}\dot{\omega}_i \times {}^{i}P_{i+1} + {}^{i}\omega_i \times ({}^{i}\omega_i \times {}^{i}P_{i+1}) + {}^{i}\dot{v}_i\right] \tag{3} $$

where ${}^{i+1}_{i}R$ is the rotation matrix between the i^{th} and $(i+1)^{th}$ link, $\times$ represents the cross product operation, ${}^{i}P_{i+1}$ is the position vector of frame $i+1$, which is the upper right 3×1 vector of the D-H matrix. The rotation matrices R, can be obtained by taking the transpose of the upper left 3×3 transformation matrix and the D-H parameters shown in Table I. The single and double dot notation represents the first and second derivatives with respect to time. We initialize $\omega_0 = \dot{\omega}_0 = (0,0,0)^T$. Effect of gravity is included in the model at no extra cost by setting $\dot{v}_0 = (g_x, g_y, g_z)^T$, where g is gravity along each of the three axes. These forward recursive equations are used to propagate angular velocity, and angular and linear acceleration from the reference coordinate system through the links of upper arm, forearm and wrist.

C. State Space Model

The general discrete time state-space model is of the form,

$$ x(n+1) = f_n\left[x(n), u(n)\right] \tag{4} $$

$$ y(n) = h_n\left[x(n), v(n)\right] \tag{5} $$

where $x(n)$ is the unobserved state of the system, $y(n)$ is the observed or measured data, $f_n[\cdot]$ and $h_n[\cdot]$ are nonlinear state and observation equations, $u(n)$ and $v(n)$ are the state and observation white noise with zero mean. Our state model equations which describe the evolution of the states with time are given by

$$ \theta_i(n+1) = \theta_i(n) + T_{\mathrm{s}}\dot{\theta}_i(n) + \tfrac{1}{2}T_{\mathrm{s}}^2\ddot{\theta}_i(n) \tag{6} $$

$$ \dot{\theta}_i(n+1) = \dot{\theta}_i(n) + T_{\mathrm{s}}\ddot{\theta}_i(n) \tag{7} $$

$$ \ddot{\theta}_i(n+1) = \alpha\ddot{\theta}_i(n) + u_{\ddot{\theta}_i}(n) \tag{8} $$

where $i = \{1, \ldots, 6\}$ of the six angles, $\theta_i(n)$ is the i^{th} angle at time n, $\dot{\theta}_i$ is the angular velocity, $\ddot{\theta}_i$ is the angular acceleration, $u_{\ddot{\theta}_i}(n)$ is a white noise process with zero mean, α is a process model parameter, and $T_{\mathrm{s}} = 1/f_{\mathrm{s}}$ is the sampling period. These are standard equations for a physical object traveling at a constant acceleration. The model assumes the acceleration is constant for the duration of a sampling interval. This is sufficient for our data, which was acquired with a sample rate of $f_{\mathrm{s}} = 128$ Hz. The angular acceleration is modeled as a first-order autoregressive process with zero mean. Depending on the choice of the parameter α, this represents process models ranging from a random walk model ($\alpha = 1$) to a white noise model ($\alpha = 0$). For values of $\alpha < 1$ the estimated angular accelerations are biased towards 0. Typically, the value of α is assigned an intermediate value that represents typical patterns of constrained human joint rotation, which does not grow unbounded. It is one of the filter parameters tuned to improve the tracking performance. Its value and other parameter used in the tracker are described in Table II.

The observation model describes the measurement obtained by the triaxial gyroscope for the angular rate and the triaxial accelerometer for the translational acceleration

$$ y(n) = \begin{bmatrix} \omega(\mathbf{n}) \\ \dot{\mathbf{v}}(\mathbf{n}) \end{bmatrix} + \begin{bmatrix} \mathbf{v_g}(\mathbf{n}) \\ \mathbf{v_a}(\mathbf{n}) \end{bmatrix} $$

where $\omega = \{\omega_x, \omega_y, \omega_z\}^T$ is the angular velocity along the X, Y and Z axes. The gyroscope noise is described by the 3D vector $\mathbf{v_g}$. Similarly, the translational accelerations and their noise along the three axes are $\dot{\mathbf{v}} = \{\dot{v}_x, \dot{v}_y, \dot{v}_z\}^T$. It should be noted that the acceleration measurement vector includes translational accelerations and the effect gravity.

D. Modeling Sensor Random Drift

To reduce the effect of random drift on shoulder rotation angle estimates, we model the bias of the sensors placed on the shoulder. Bias is modeled as a random walk, adding 6 more dimensions to the process model:

$$\begin{aligned}\theta_i(n+1) &= \theta_i(n) + T_s\dot{\theta}_i(n) + \tfrac{1}{2}T_s^2\ddot{\theta}_i(n)\\ &\vdots\\ \mathbf{b}_\omega(n+1) &= \mathbf{b}_\omega(n) + \mathbf{u}_{\mathbf{b}\omega}(n)\\ \mathbf{b}_\mathbf{a}(n+1) &= \mathbf{b}_\mathbf{a}(n) + \mathbf{u}_{\mathbf{ba}}(n)\end{aligned}$$

The 3D gyroscope bias $\mathbf{b}_\omega$ and 3D accelerometer bias $\mathbf{b}_\mathbf{a}$ are random walk with zero-mean white noise $\mathbf{u}_{\mathbf{b}\omega}$ and $\mathbf{u}_{\mathbf{ba}}$. The observation equation for the inertial measurement unit placed on the upper arm is given below:

$$\omega_x(n) = \dot{\theta_1}\cos(\theta_2) + b_{\omega x} \tag{9}$$

$$\omega_y(n) = -\dot{\theta_1}\sin(\theta_2) + b_{\omega y} \tag{10}$$

$$\omega_z(n) = \dot{\theta_2} + b_{\omega z} \tag{11}$$

$$\begin{aligned}\dot{v}_x(n) = {} & a_1\sin(\theta_2)\dot{\theta_1}^2 + g\cos(\theta_2) - \dot{\theta_1}^2 a_2\sin(\theta_2)^2\\ & - \dot{\theta_2}^2 a_2 + b_{ax}\end{aligned} \tag{12}$$

$$\begin{aligned}\dot{v}_y(n) = {} & a_1\cos(\theta_2)\dot{\theta_1}^2 - g\sin(\theta_2) - \dot{\theta_1}^2 a_2\cos(\theta_2)\sin(\theta_2)\\ & + \ddot{\theta_2}a_2 + b_{ay}\end{aligned} \tag{13}$$

$$\begin{aligned}\dot{v}_z(n) = {} & a_1 a_2\cos(\theta_2)\dot{\theta_1}\dot{\theta_2} + \ddot{\theta_1}a_2\sin(\theta_2)\\ & + \dot{\theta_1}\dot{\theta_2}a_2\cos(\theta_2) - a_1\ddot{\theta_1} + b_{az}\end{aligned} \tag{14}$$

where θ_i is the i^{th} angle at time n, $\dot{\theta}_i$ is the angular velocity, and $\ddot{\theta}_i$ is the angular acceleration. The distance between elbow flexion joint and the device is a_2. The time index n was dropped from right-side of the equations for ease of readability. Observation equations for the forearm and wrist sensors are too large to be shown here.

E. Anatomical Constraints in The Shoulder And Elbow

The state model equations provide an elegant and convenient mean of incorporating prior knowledge of physical constraints on state estimates to obtain accurate estimation. Human shoulder rotation around the humerus bone cannot exceed $90°$. Similarly, shoulder cannot attain more than $180°$ of abduction or flexion [32]. The natural range of elbow flexion is between zero and $145°$. The range of forearm supination is between zero and $85°$, and between zero and $80°$ for the forearm pronation. The wrist flexion/extension natural range is $\pm 75°$. There are many ways to incorporate state constraints into the nonlinear state estimators [33]. In this study, the constraints information are incorporated in the UKF algorithm during the time update, by restricting the sigma points within the natural range of motion region. The constrained sigma points are then used to in the measurement update, Kalman gain calculation, and state updates. During the measurement update, the constraints may be violated due to the linearization. However, these violations are rare and small in magnitude.

F. Zero-Velocity Updates

To mitigate the effect of gyroscope drift on the estimated heading angles during long periods of movement, we employ the zero-velocity updates. Zero-velocity updates has been used in ambulatory gait analysis and pedestrian navigation. During walking cycles, human feet alternate between a moving stride phase and a stationary stance phase when the foot is on the ground. In their tracking algorithm, Feliz *et al.* detected the stationary phase when the total angular rate was below $1^{rad}/\sec$ [34] to reset the angular rate to zero. Resetting the inertial data to zero is referred to as hard update. Foxlin detected the stationary phase when gyroscope and accelerometer data stayed below a prescribed threshold for at least 0.15 seconds. He applied zero-velocity updates as pseudo-measurements in an EKF navigation error corrector [35]. This is classified as soft zero-velocity updates [36]

In this study, we only apply zero-velocity to update estimates of the gyroscope bias around the vertical axis. Since our algorithm uses gravity to estimate the attitude and we only lack an absolute reference for heading about the vertical axis. When the rotational rate around the vertical axis stays below $3°/\sec$ for at least $0.25\sec$, movement is considered static. During this static period, the measurement equation is augmented with a pseudo-measurement of gyroscope vertical axis random bias. Putting pseudo-measurements into the UKF filter, instead of applying a hard update by resetting the velocity to zero, provides additional benefits. Firstly, the filter provides an estimate of the gyroscope bias, and corrects rotational rate estimates. Thus, the filter corrects estimates of heading angle, and consequently other distal arm angles.

G. Nonlinear state estimator

The model introduced above has a nonlinear relationship between the angles and sensor measurements. The EKF is the most common method of nonlinear state estimation. It is based on linearizing the state and observation models with a first-order Taylor series expansion. It models the state variables with first and second order moments, which is most appropriate when the distribution is Gaussian. The linearization leads to poor performance if the dynamics are highly nonlinear and the local linearization insufficiently characterizes the relationship. The EKF also requires calculation of Jacobian matrices, which can be difficult, tedious, error prone, and time consuming.

Sequential Monte Carlo methods, also known as particle filters, can overcome the performance and implementation limitations of the EKF [37]. These algorithms can be applied to highly nonlinear and non-Gaussian estimation problems, but they have computational requirements that are often orders of magnitude larger than the EKF or UKF. The UKF has nearly the same computational requirements as the EKF, but uses a more accurate method to characterize the propagation of the state distribution through the nonlinear models [38]. While the methods described in this article could be implemented with any of these nonlinear state space tracking algorithms, in our tracker we used the UKF. We also implement the tracker with the EKF to compare its performance versus UKF.

Q and R, are user-specified parameters to represent the process and the measurement noise covariance. Since we assume

white Gaussian noise, we set the off-diagonal entries of the two matrices to zeros. The diagonal elements of R are determined empirically and account for the uncertainty in the measurement data. We approximate the measurement noise based on short static periods at both ends of sensor measurements. Q is the process noise covariance matrix, and its diagonal elements are used as tuning parameters. These parameters control the tradeoff between certainty in the process model representing accurate motion dynamics, and how precisely the model tracks the sensor measurements. Table II lists the different parameters used to generate the tracking results.

TABLE II
USER-SPECIFIED PARAMETERS AND SAMPLE RATE FOR THE UKF- AND EKF-BASED TRACKER. I REPRESENTS AN IDENTITY MATRIX.

Name	Symbol	Value
Variance of gyroscope measurement white Gaussian noise	${\sigma_{v_g}}^2$	.0001
Variance of accelerometer measurement white Gaussian noise	${\sigma_{v_a}}^2$	.0064
Variance of process white Gaussian noise	${\sigma_u}^2$	1.00
Initial state covariance matrix	P	I
Angular acceleration process parameter	α	0.90

H. Performance assessment

To evaluate the performance of the inertial tracking system in monitoring arm movement, we compared the joint angles calculated by the inertial tracker with those obtained from an industrial Epson C3 robot arm (Epson Robots, California) with six degrees of freedom. The arm is a high speed, and a very high precision industrial robot, that is normally used for medical device and parts assembly. Three Opal sensors (APDM, Portland, OR), each containing triaxial accelerometers and gyroscopes were placed on the upper arm, forearm and wrist as shown in Fig. 2. Table III shows the Epson C3 range of motion and operating speed of the six joints.

TABLE III
MAXIMUM OPERATING SPEED AND MOTION RANGE FOR THE ROBOT ARM.

Task	Rate	Max. Motion Range
Shoulder Internal/External Rotation	$450°/\,\text{sec}$	$\pm 180°$
Shoulder Flexion/Extension	$450°/\,\text{sec}$	$-160°\ , +65°$
Elbow Flexion/Extension	$514°/\,\text{sec}$	$-51°\ , +225°$
Forearm Supination/Pronation	$553°/\,\text{sec}$	$\pm 200°$
Wrist Flexion/Extension	$553°/\,\text{sec}$	$\pm 135°$
Wrist Twist	$720°/\,\text{sec}$	$\pm 360°$

Inertial sensor and robot data were synchronized by calculating the lag time using cross-correlation analysis.

$$\hat{r}_{yx}(\ell) \approx \mathrm{E}[y(n)x(n-\ell)] \tag{15}$$

If $\max(\hat{r}_{yx})$ is significant at lags $|\ell| > 0$, then ℓ gives information about the delay between the signals. In this study, inertial sensors were started before the robot arm. Hence, the robot data was lagging. The lagging robot data was augmented with ℓ zeros to synchronize it with the leading sensor data.

The majority of the tracking algorithms discussed in the introduction limit their performance assessment to movement performed with slow articulation. To verify the performance of our inertial algorithm in tracking normal and fast movement, we collected planar and complex arm movement at three different rotational rates. The first data set was of the arm movement at slow speed, which was defined as one fourth of the arm maximum rotational rate. The second and third data sets were of the arm movement at medium and fast speed, which were defined as one half and full range of the maximum arm rotational rate, respectively.

Another limitation of previous systems, is the brief time duration of correct tracking or assessment. In this study, each data set lasted at least15 minutes. Each recording started with a stationary period of 3 seconds at the initial pose. This period was used to estimate the gyroscope deterministic bias offset. The mean of each gyroscope-axis stationary measurement was removed from gyroscope data before calculating the joint angles. The rest of the recording was designed to include simple planar movement around each of the six joints. Each planar movement, explained in Table III, was repeated four times. This was followed by a second of stationary movement, and ended with a complex joints movement that involved the three joint simultaneously to mimic regular arm movement for about two minutes. This arm trajectory was repeated a few times to obtain 3 continuous 15-minute recordings of robot arm movements at slow, medium and fast rotation rate.

III. RESULTS

We used two different trackers to compare the performance of the EKF to that of the UKF in estimating the joint angles. The assessment of the tracking performance is based on the entire 15-minute duration of recording of arm movement.

A. Baseline Performance Results

In this section, we present baseline performance results of the tracker before employing the modified model to account for sensor drift, physical constraints and zero-velocity updates. The baseline results will be used to assess the performance improvement introduced by employing the drift reduction techniques. We calculated the correlation coefficient r, and the average root mean squared error (RMSE) between angle estimates from the inertial tracker and true arm angles. Table IV shows the baseline RMSE for the three data sets.

TABLE IV
BASELINE RMSE BETWEEN TRUE ROBOT ANGLES AND ESTIMATED USING THE UKF OF THE THREE DATA SETS.

Task	Slow (°)	Medium (°)	Fast (°)
Shoulder Internal/External Rotation	25.0	8.1	9.6
Shoulder Flexion/Extension	1.1	2.4	2.5
Elbow Flexion/Extension	1.1	2.6	3.3
Forearm Supination/Pronation	1.4	2.1	2.4
Wrist Flexion/Extension	1.2	2.2	2.9
Wrist Twist	1.8	3.9	3.8
Rotational Rate	$\leq 180\ °/\text{s}$	$\leq 360\ °/\text{s}$	$\leq 720\ °/\text{s}$

B. UKF Performance with Modified Arm Model

We combined the three techniques discussed above into one modified arm model to account for sensor drift, and to employ physical constraints and zero-velocity updates. Fig. 3 show the last two minutes of the wrist true angles (dotted red lines) and their estimates (solid blue lines) using the UKF-based inertial tracking system during slow rotation rate up to $180°/\,\text{sec}$. Fig. 4 shows the last two minutes of shoulder internal/external rotation, and flexion/extension angles and

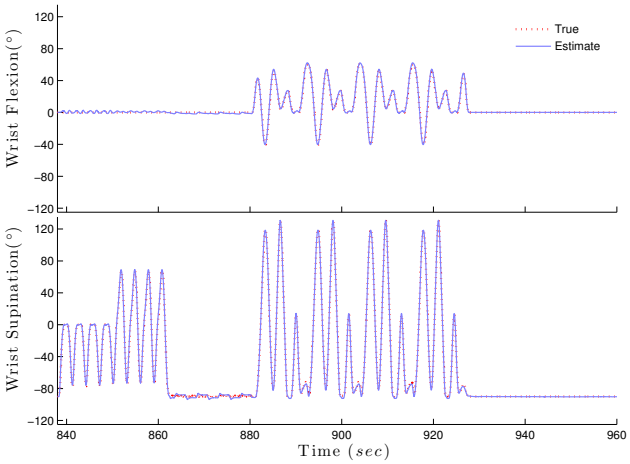

Fig. 3. True (dotted red line) and estimated (solid blue line) wrist angles during the last 2 minutes of slow arm movement.

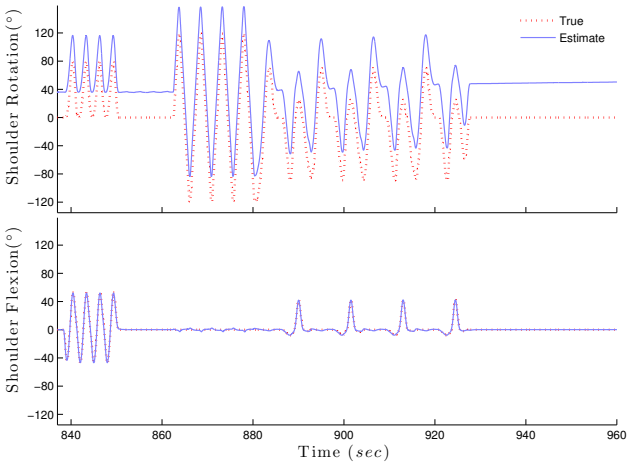

Fig. 4. Baseline shoulder angle estimates compared to the true angles during the last 2 minutes of slow arm movement.

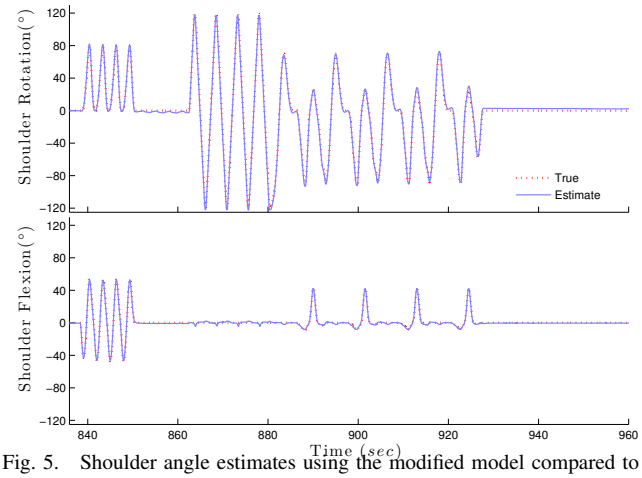

Fig. 5. Shoulder angle estimates using the modified model compared to the true angles during the last 2 minutes.

their baseline estimates during slow rotation. Fig. 5 shows the same angles estimated using the modified model.

Table V shows that the new modified model dramatically decreased shoulder internal/external rotation angle error from 25.0° to 7.8°; an error reduction of 69% compared to baseline estimates around the vertical axis. The modified model also resulted in an increased average correlation

TABLE V
RMSE BETWEEN ANGLE ESTIMATES AND TRUE ROBOT ARM ANGLES DURING SLOW, MEDIUM AND FAST SPEED MOVEMENT USING UKF.

Task	Slow (°)	Medium (°)	Fast (°)
Shoulder Internal/External Rotation	7.8	3.0	5.9
Shoulder Flexion/Extension	0.8	1.6	2.5
Elbow Flexion/Extension	0.9	2.0	2.8
Forearm Supination/Pronation	1.3	1.2	1.1
Wrist Flexion/Extension	1.1	1.5	1.8
Wrist Twist	1.7	2.8	2.2
Error reduction	69%	63%	39%

from 0.92 to 0.98 for slow movement. Consistent with the results for slow arm movement, tracking errors between inertial angle estimates and true robot joint angles were $\leq 3.0°$ during medium-speed movement, and $\leq 5.9°$ during fast-speed movement. Error in shoulder internal/extension rotation estimates was still higher than the joint angle error, although it dropped from 8.1° to 3.0° during medium movement, and from 9.6° to 5.9° during fast movement. Error in the other five arm angles were consistently lower that estimation error the shoulder rotation, with a maximum error of 2.8° in elbow flexion/extension during fast arm movement.

C. EKF Performance

We implemented the inertial tracker with the EKF using the modified arm model, and the same user-specified parameters which were used with the UKF-based tracker. Fig. 6 shows the last two minutes of the robot shoulder during medium internal/external rotation around the vertical axis at a rotational rate of $225°/\text{sec}$. We obtained consistent agreement between the true arm angles and their inertial estimates.

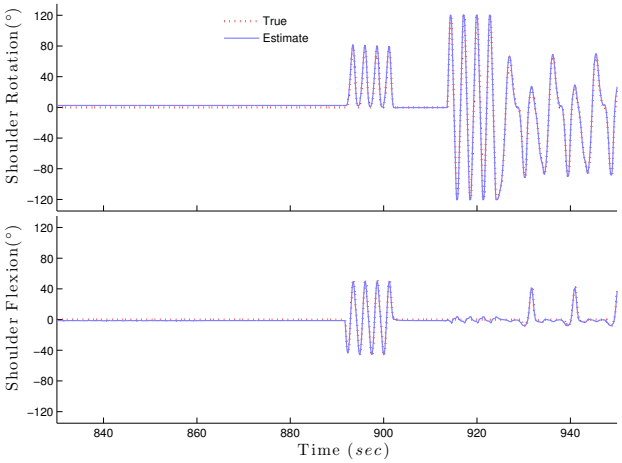

Fig. 6. True shoulder angles and their estimates of the last 2 minutes at an average rotation rate of 225 °/s. Angles were estimated using the modified arm model with the EKF-based tracker.

TABLE VI
RMSE BETWEEN ANGLE ESTIMATES AND TRUE ROBOT ARM ANGLES DURING SLOW, NORMAL AND FAST SPEED MOVEMENT USING EKF.

Task	Slow	Regular	Fast
Shoulder Internal/External Rotation	8.8	8.6	9.7
Shoulder Flexion/Extension	1.2	1.9	2.5
Elbow Flexion/Extension	1.3	2.1	3.1
Forearm Supination/Pronation	0.8	1.4	1.4
Wrist Flexion/Extension	1.2	1.9	2.9
Wrist Twist	1.8	3.7	3.4

IV. Discussion

In this study, we combined kinematic models with state space methods to estimate human joint angles using wearable inertial measurement units. The state model equations provide elegant and efficient means of incorporating sensor bias model, prior knowledge of physical constraints on state estimates, and zero-velocity updates to obtain accurate estimation of continuous long recordings. Besides the rotational rate data, the state space model includes both the translational and gravitational components of acceleration. This enables the system to provide state estimates during both fast and slow movements with consistent accuracy. States estimates included joint angles, angular rotation and acceleration. This framework could easily be extend to estimate joint segment lengths and segment positions, to provide full human body kinematics during spontaneous daily activities.

We used the unscented Kalman filter (UKF) to estimate shoulder, elbow and wrist joint angles from an industrial robot arm with 6 DOFs. Despite the different characteristics of human movement from the movement of robots, we argue that using a robot arm for assessment has many advantages over the traditional optical systems. The different characteristics are mainly due to the type of joints. According to [32], the human arm mechanism is composed of 7 DOFs, with shoulder joint as a ball-and-socket joint with 3 DOFs. However, the robot shoulder has only 2 DOFs, which limits the comparison to only 6 DOFs. Despite this limitation, using the robot arm for assessment provides many advantages. Unlike motion capture systems, which require estimation of joint angles from marker positions and interpolation during marker occlusions, the robot system provides direct angle measurements with high precision. The arm movement rate can be controlled to a desired rate ranging from slow to very fast, up to $720^\circ/\sec$. The robot provides a wide range of motion that can easily mimic human movement in performing various tasks.

A stationary calibration period of 3 seconds at the initial pose preceded each data set served multiple purposes. The first was to align the inertial sensors and the robotic reference system. The second was to calculate the variance of sensor measurement noise. The stationary period was also used to calculate the gyroscope constant bias. This bias was removed from the gyroscope data before calculating the joint angles.

Compared to joint angles obtained from the robot reference system, we achieved an average RMS angle error $\leq 3^\circ$ during slow arm movement at a rotational rate $\leq 180^\circ/\sec$. As expected, a maximum error of 7.8° was obtained for heading angles around the vertical axis. Estimation error accumulates around the vertical axis during slow or static periods. In absence of changes in acceleration, gravity alone does not provide any complementary data to that of the gyroscope. Shoulder angle estimates around the vertical axis rely only on gyroscope data, therefore error accumulates due to gyroscope drift after 15 minutes. This, however, is a very reasonable error range compared to what was reported by Roetenberg who showed that integration of noisy gyroscope data resulted in a drift between 10–25° after one minute [12].

In contrast to many studies discussed in the introduction, we validated the performance of our tracking algorithm during different speeds, over 15 minutes. Angle estimates during arm movement at medium rotation rate $\leq 360^\circ/\sec$ are very similar to those obtained during slow movement. On average, the RMS angle error was 2.0°, with a maximum error of 3.0° between true and estimated shoulder internal/external rotation. The error slightly increased during fast movement with an average RMS angle error of 2.7°, and a maximum error of 5.9° between true and estimated shoulder internal/external rotation. Besides the effect of gyroscope drift on the accuracy of the estimated angles, there was another source of noise that contributed to the larger error. That was the effect of fast arm movement on the table on which the arm is mounted. Due to the very fast movement, the table was vibrating strongly, especially during rotation around the vertical axis, adding more noise to the sensor measurements. Despite the slightly higher estimate error during fast movement, we maintained a very reasonable error range compared to what was achieved by other studies which reported error range of $12^\circ - 16^\circ$ [25].

The combined effect of imposing physical constraints, modeling sensor bias, and employing zero-velocity updates resulted in a considerable decrease in tracking error. The RMSE dropped from 25.0° of the baseline heading angle to 7.8° for estimates during slow rotation; an error reduction of 69%. Similarly, the RMSE dropped from 8.1° with the baseline heading angle to 3.0°; an error reduction of 63% for joint angles during medium-speed rotation. Estimation error of fast shoulder rotation around the vertical axis was reduced also from 9.6° to 5.9°. The combined effect of using the modified model in reducing the error due to sensor drift can be observed especially during the last few minutes of the recording in Fig. 4. With the prior knowledge that the arm rotation cannot exceed a certain limit, the effect of gyroscope drift on angle estimates was reduced to a very reasonable range of errors. This eliminates the need to using magnetic sensors which leads to large errors due to magnetic field disturbances [25].

Results for the EKF-based tracker shows that the UKF performs slightly better. On average, the RMSE was $2.5^\circ, 3.3^\circ$, and 3.8° during slow, regular and fast arm movement respectively. As in the UKF case, maximum error was obtained for heading angles around the vertical axis. Shoulder internal/external rotation ranged from 8.6° to 9.7°. The additional complexity of the EKF in deriving a Jacobian matrix, besides the UKF better performance, leads to the conclusion that the UKF is a better choice for estimating Joint angles.

Natural resting positions of the human arm could be detected, and used to correct long-term drift during the day. We are currently collecting continuous data from human subjects performing daily life activities. We plan to study the effect of employing drift-correction to shoulder joint angles during these resting positions.

V. Conclusion

The results presented here demonstrate that wearable inertial sensors have the potential to achieve a level of accuracy that facilitates the study of normal and pathological human movement. We combined kinematic models designed for control of

robotic arms with state space methods to directly and continuously estimate human joint angles using wearable inertial sensors. These algorithms can be applied to any combination of synchronized sensors and can be generalized to track any limb movement. The state space framework enables one to efficiently impose physical constraints on state estimates, and to track in real-time or with improved accuracy offline. The agreement with a high-precision robot arm reference system was excellent. Unlike other motion systems, which require fixed cameras in a controlled environment and suffer from problems of occlusion, wearable inertial sensors can be used anywhere, cannot be occluded, and are low cost. Our proposed method used a minimal sensor configuration with one sensor on each segment. In addition, our method is very accurate during long periods of movements at various rotational rates.

REFERENCES

[1] H. Graichen, S. Hinterwimmer, R. von Eisenhart-Rothe, T. Vogl, K. Englmeier, and F. Eckstein, "Effect of abducting and adducting muscle activity on glenohumeral translation, scapular kinematics and subacromial space width in vivo," *J Biomech.*, vol. 38, no. 4, pp. 755–760, 2005.

[2] R. J. de Asla, L. Wan, H. E. Rubash, and G. Li, "Six DOF in vivo kinematics of the ankle joint complex: Application of a combined dual-orthogonal fluoroscopic and magnetic resonance imaging technique," *Journal of Orthopaedic Research*, vol. 24, pp. 1019–1027, May 2006.

[3] M. J. Bey, S. K. Kline, R. Zauel, T. R. Lock, and P. A. Kolowich, "Measuring Dynamic In-Vivo Glenohumeral Joint Kinematics: Technique And Preliminary Results," *Journal of Biomechanics*, vol. 41, no. 3, pp. 711–714, November 2008.

[4] J. B. Lunden, J. P. Braman, R. F. LaParade, and P. M. Ludewig, "Measuring Dynamic In-Vivo Glenohumeral Joint Kinematics: Technique And Preliminary Results," *Journal of Shoulder and Elbow Surgery*, vol. 19, no. 2, pp. 216–223, March 2010.

[5] C. E. Draper, T. F. Besier, M. Fredericson, J. M. Santos, G. S. Beaupre, S. L. Delp, and G. E. Gold, "Differences in patellofemoral kinematics between weight-bearing and non-weight-bearing conditions in patients with patellofemoral pain," *Journal of Orthopaedic Research*, vol. 29, no. 3, pp. 312–317, March 2011.

[6] E. Roux, S. Bouilland, A. Godillon-Maquinghen, and D. Bouttens, "Evaluation of the global optimization method within the upper limb kinematics analysis," *J Biomech.*, vol. 35, no. 9, pp. 1279–1283, 2002.

[7] G. Welch and E. Foxlin, "Motion Tracking: No Silver Bullet, but a Respectable Arsenal," *IEEE Computer Graphics and Applications*, vol. 22, no. 6, pp. 24–38, Nov-Dec 2002.

[8] K. Liu, T. Liu, K. Shibata, Y. Inoue, and R. Zheng, "Novel approach to ambulatory assessment of human segmental orientation on a wearable sensor system," *Journal of Biomechanics*, vol. 42, no. 16, pp. 2747–2752, September 2009.

[9] F. Bagal, V. L. Fuschillo, L. Chiari, and A. Capello, "Calibrated 2D angular kinematics by single-axis accelerometers: From inverted pendulum to N-Link chain," *IEEE Sensors Journal*, vol. 12, no. 3, pp. 479–486, March 2012.

[10] H. Dejnabadi, B. M. Jolles, E. Casanova, P. Fua, and K. Aminian, "Estimation and Visualization of Sagittal Kinematics of Lower Limbs Orientation Using Body-Fixed Sensors," *IEEE Transactions on Biomedical Engineering*, vol. 53, no. 7, pp. 1385–1393, July 2006.

[11] J. Bregmann, R. Mayagoitia, and I. Smith, "A portable system for collecting anatomical joint angles during stair ascent: a comparison with an optical tracking device," *Dynamic Medicine*, vol. 8, no. 3, 2009.

[12] D. Roetenberg, "Inertial and Magnetic Sensing of Human Motion," Ph.D. dissertation, University of Twente, The Netherlands, 2006.

[13] D. Roetenberg, H. Luinge, C. Baten, and P. Veltink, "Compensation of magnetic disturbances improves inertial and magnetic sensing of human body segment orientation," *IEEE Transactions on Neural Systems and Rehabilitation Engineering*, vol. 13, no. 3, pp. 395–405, 2005.

[14] K. O'Donovan, R. Kamnik, D. O'Keeffe, and G. Lyons, "An inertial and magnetic sensor based technique for joint angle measurement," *Journal of Biomechanics*, vol. 40, no. 16, pp. 2604–2611, March 2007.

[15] W. H. K. de Vries, H. E. J. Veeger, A. G. Cutti, C. Baten, and F. C. T. van der Helm, "Functionally interpretable local coordinate systems for the upper extremity using inertial and magnetic measurement systems," *Journal of Biomechanics*, vol. 43, pp. 1983–1988, 2010.

[16] J. Favre, B. M. Jolles, R. Aissaoui, and K. Aminian, "Ambulatory measurement of 3D knee joint angle," *Journal of Biomechanics*, vol. 41, no. 5, pp. 1029–1035, January 2008.

[17] H. Luinge, P. Veltink, and C. Baten, "Ambulatory Measurement of Arm Orientation," *Journal of Biomechanics*, vol. 40, pp. 78–85, 2007.

[18] H. Luinge, D. Roetenberg, and P. Slycke, "Motion tracking system," U.S. Patent 2008/0285805 A1, November 2008.

[19] G. Cooper, L. Sheret, and L. *et al.* . McMillan, "Inertial sensor-based knee flexion/extension angle estimation," *Journal of Biomechanics*, vol. 42, no. 16, pp. 2678–2685, 2009.

[20] E. R. Bachmann and R. B. McGhee, "Inertial and magnetic posture tracking for inserting humans into networked virtual environments," in *ACM Symposium on Virtual Reality Software and Technology*. ACM: New York, NY, 2001, pp. 9–16.

[21] H. Zhou and H. Hu, "Inertial motion tracking of human arm movements in stroke rehabilitation," in *Proceedings of the IEEE International Conference on Mechatronics and Automation*, 2005, pp. 1306–1311.

[22] X. Yun and E. Bachmann, "Design, Implementation, and Experimental Results of a Quaternion-Based Kalman Filter for Human Body Motion Tracking," *IEEE Transaction on Robotics*, vol. 22, pp. 1217–1227, 2006.

[23] D. Roetenberg, P. Slycke, and P. Veltink, "Ambulatory Position and Orientation Tracking Fusing Magnetic and Inertial Sensing," *IEEE Transactions on Biomedical Engineering*, vol. 54, no. 5, pp. 883–890, May 2007.

[24] H. Zhou and H. Hu, "Upper limb motion estimation from inertial measurements," *International Journal of Information Technology*, vol. 13, no. 1, pp. 1–14, 2007.

[25] E. R. Bachmann, X. Yun, and C. Peterson, "An investigation of the effects of magnetic variations on Inertial/Magnetic orientation sensors," in *Proceedings of the 2004 IEEE International Conference on Robotics and Automation*, 2004, pp. 1115–1122.

[26] X. Yun, E. Bachmann, and R. McGhee, "A Simplified Quaternion-Based Algorithm for Orientation Estimation From Earth Gravity and Magnetic Field Measurements," *IEEE Transactions on Instrumentation and Measurement*, vol. 57, no. 3, pp. 638–650, 2008.

[27] A. G. Cutti, A. Giovanardi, L. Rocchi, A. Davalli, and R. Sacchetti, "Ambulatory measurement of shoulder and elbow kinematics through inertial and magnetic sensors," *Medical & biological engineering & computing*, vol. 46, pp. 169–178, February 2008.

[28] M. El-Gohary and J. McNames, "Shoulder And Elbow Joint Angle Tracking with Inertial Sensors," *IEEE Transactions on Biomedical Engineering*, vol. 59, no. 9, pp. 577–585, July 2012.

[29] A. G. Cutti, C. Troncossi, A. Davalli, and R. Sacchetti, "Soft tissue artefact assessment in humeral axial rotation," *Gait Posture*, vol. 21, pp. 341–349, April 2005.

[30] J. J. Craig, *Introduction to Robotics, Mechanics and Control*, ser. Electrical and Computer Engineering: Control Engineering. Addison-Wesley, 1989.

[31] M. El-Gohary, L. Holmstrom, J. Huisinga, E. King, and J. McNames, "Upper limb joint angle tracking with inertial sensors," in *Engineering in Medicine and Biology Society, EMBC, 2011 Annual International Conference of the IEEE*, 2011, pp. 5629–5632.

[32] A. Forner-Cordero, J. L. Pons, E. A. Turowska, and A. Schiele, "Kinematics and dynamic of wearable robots," in *Wearable Robots: Biomechatronic Exoskeletons*, 2nd ed., J. L. Pons, Ed. West Sussex, England: John Wiley & Sons Ltd, 2008, ch. 3, pp. 47–85.

[33] D. Simon, "Kalman filtering with state constraints: a survey of linear and nonlinear algorithms," *Control Theory & Application*, vol. 4, no. 8, pp. 1303–1318, August 2010.

[34] R. Feliz, E. Zalama, and J. G. Garcia-Bermejo, "Pedestrian tracking using inertial sensors," *Journal of Physical Agents*, vol. 3, no. 1, pp. 35–42, January 2009.

[35] E. Foxlin, "Pedestrian Tracking with Shoe-Mounted Inertial Sensors," *IEEE Computer Graphics and Applications In Computer Graphics and Applications*, vol. 25, no. 6, pp. 38–46, November 2005.

[36] I. Skog, P. Händel, J.-O. Nilsson, and J. Rantakokko, "Zero-Velocity Detection – An Algorithm Evaluation," *IEEE Transaction on Biomedical Engineering*, vol. 57, no. 11, pp. 2657–2666, November 2010.

[37] O. Cappé, S. Godsill, and E. Moulines, "An overview of existing methods and recent advances in sequential monte carlo," in *Proceedings of the IEEE*, vol. 95, May 2007, pp. 899–924.

[38] S. Julier and J. Uhlmann, "Unscented filtering and nonlinear estimation," in *Processings of The IEEE*, vol. 92, 2004, pp. 401–422.